Superconductor Science and Technology

PAPER

The interplay between anomalous metallic and superconducting states tuned by disorder in thin flakes of Kagome metal KV_3Sb_5

To cite this article: Teng Wang *et al* 2023 *Supercond. Sci. Technol.* **36** 125015

View the article online for updates and enhancements.

You may also like

- Flat band of Kagome lattice in graphene plasmonic crystals
Liqiang Zhuo, Huiru He, Ruimin Huang et al.
- Topological phases of graphene-Kagome systems
A B Felix de Souza, L Spreafico, D Faria et al.
- Superconductivity and phase transitions in Kagome compound $Pd_3P_2S_8$ from first-principles calculation
Bin Li, Yeqian Yang, Yuxiang Fan et al.

This content was downloaded from IP address 180.168.188.241 on 30/11/2023 at 05:04

IOP Publishing Superconductor Science and Technology
Supercond. Sci. Technol. **36** (2023) 125015 (8pp) https://doi.org/10.1088/1361-6668/ad06c4

The interplay between anomalous metallic and superconducting states tuned by disorder in thin flakes of Kagome metal KV_3Sb_5

Teng Wang[1,2], Aobo Yu[1,3], Yuanlv Mao[4], Yuqiang Fang[4], Yixin Liu[1,3], Han Zhang[1,3], Wang Guo[1,3], Wei Li[5], Wei Peng[1,3], Zengfeng Di[1,3], Fuqiang Huang[3,4], Da Jiang[1,6,*] and Gang Mu[1,3,*]

[1] National Key Laboratory of Materials for Integrated Circuits, Shanghai Institute of Microsystem and Information Technology, Chinese Academy of Sciences, Shanghai 200050, People's Republic of China
[2] School of Physical Science and Technology, ShanghaiTech University, Shanghai 201210, People's Republic of China
[3] University of Chinese Academy of Sciences, Beijing 100049, People's Republic of China
[4] State Key Laboratory of High Performance Ceramics and Superfine Microstructure, Shanghai Institute of Ceramics, Chinese Academy of Sciences, Shanghai 200050, People's Republic of China
[5] State Key Laboratory of Surface Physics and Department of Physics, Fudan University, Shanghai 200433, People's Republic of China
[6] Institute for Frontiers and Interdisciplinary Sciences, Zhejiang University of Technology, Hangzhou 310014, People's Republic of China

E-mail: jiangda@zjut.edu.cn and mugang@mail.sim.ac.cn

Received 28 July 2023, revised 8 October 2023
Accepted for publication 25 October 2023
Published 8 November 2023

Abstract

Recently, V-based Kagome metals have attracted intense attention due to the coexistence of their topological nontrivial electronic structure, charge density wave, and superconductivity. Here, we report the fabrication and physical investigations of single-crystalline thin flakes of the Kagome metal KV_3Sb_5. For samples with a thickness of 22 ± 2 nm, Berezinskii–Kosterlitz–Thouless type behavior is revealed by the temperature dependent resistance and voltage–current data, which indicates the presence of two-dimensional superconductivity. Meanwhile, a temperature-independent resistance behavior is observed in a wide field region, supplying the hallmark of the anomalous metallic (AM) state. Importantly, by comparing the interplay between the superconducting and AM states of two samples with different levels of disorder, a striking competitive evolution with the external field between these two states is uncovered.

Supplementary material for this article is available online

Keywords: anomalous metallic state, Berezinskii–Kosterlitz–Thouless transition, two-dimensional superconductivity, Kagome metal, KV_3Sb_5

(Some figures may appear in colour only in the online journal)

* Authors to whom any correspondence should be addressed.

 © 2023 IOP Publishing Ltd

1. Introduction

Superconducting (SC) materials have potential applications in current transmission, weak magnetic signal detection, and even quantum computing. In recent years, two-dimensional (2D) superconductivity has drawn great interest due to the emergence of new quantum phenomena, including Ising superconductivity [1–4], anomalous metallic (AM) state [5–10], Berezinskii–Kosterlitz–Thouless (BKT) transition [11–13], and even the significant enhancement of T_c [14–17]. The AM state, represented by a temperature-independent non-zero resistance at low temperature, is usually closely related to the SC state, which emerges after 2D superconductivity is suppressed by an external magnetic field or disorder. Different theories have been proposed to interpret this exotic state at low temperatures. Shimshoni *et al* attributed such a dissipative behavior to the temperature-independent quantum tunneling of vortices [18]. On the other hand, a Bose metallic phase, where the interacting Cooper pairs form a gapless non-superfluid liquid, was also proposed [5, 19]. Experimentally, investigating the relationship between SC and AM states will provide very important information for further understanding this mysterious electronic state.

Materials with a Kagome lattice manifest abundant exotic quantum phenomena including geometric spin frustration, non-trivial topological states, charge and spin density wave orders, etc [20–22]. Recently, the V-based Kagome metal, AV_3Sb_5 (A = K, Rb, Cs), has attracted intense attention due to the coexistence of topological nontrivial electronic structure, charge density wave, and superconductivity [23–26]. Theoretically the unconventional pairing in this material has been proposed considering the proximity to the multiple van Hove singularities of the SC state [27]. On the experimental side, the double-dome-shaped evolution of the SC transition temperature T_c with pressure has been confirmed by several groups [28–31]. The observation of a zero-bias conductance peak inside the vortex core indicates the possibility for Majorana bound states [32]. Moreover, the twofold symmetry of superconductivity and the anti-phase oscillation of c-axis resistivity in the normal state with respect to the in-plane magnetic field are also observed [33]. These experimental results initially show the signs of unconventional superconductivity and fertile physics in this system. Considering the layered crystal structure [23] and the tunable SC properties [34] of this material, AV_3Sb_5 supplies a suitable platform to study the nature of superconductivity in low dimensions, especially the interplay between the SC and AM states.

In this paper, we report the mechanical exfoliation and SC properties of thin flakes of KV_3Sb_5. The onset transition temperature T_c^{onset} is enhanced significantly in the thin samples ($\sim 22 \pm 2$ nm) as compared with the bulk material. Two-dimensional superconductivity is revealed by the BKT-type resistance transition. Strikingly, a transition from the SC to AM state induced by the perpendicular magnetic field is observed at low temperatures. The competitive evolution between the SC and AM states with magnetic field is revealed by comparing the behavior of two samples with different levels of disorder.

2. Experimental details

The KV_3Sb_5 single crystals were grown by the self-flux method [23]. The detailed growth process is stated in the SI. Utilizing the characteristics of the layered structure as shown in figure 1(a), the mechanical exfoliation method was adopted to fabricate the thin flakes of this material [35, 36]. Superconductivity can be observed in the samples that are thicker than about 15 nm.

The crystal structure of the KV_3Sb_5 single crystals were examined by a DX-2700-type x-ray diffractometer using Cu K_α radiation. The thicknesses and surface morphologies of the films were measured by AFM (AFM, Bruker Dimension Icon). The surface morphologies of the samples were measured by scanning electron microscopy (SEM, Zeiss Supra55). The sample quality was also evaluated using a Raman spectrometer (Horiba LabRAM HR Evolution).

The electrical resistance and voltage–current curves were collected on the dilution refrigerator based on the physical property measurement system (Quantum Design, PPMS) by a standard four-probe method, and the silver paste was used to fabricate the electrodes. The contact resistance is in the order of tens of Ohms. RC filters were used to filter the external radiation effectively. External magnetic field was applied perpendicular to the sample surface and the electric current. The applied electric current is in the range of 5–10 μA. Sample S-1 was not specially protected, while sample S-2 was protected by epoxy after the fabrication of electrodes (see figure 1(c)). The exposure time to air of samples S-1 and S-2 was nine and two minutes, respectively.

3. Results

3.1. Characterization

As shown in figure 1(a), KV_3Sb_5 shows a Kagome structure with the space group of *P6/mmm*. The x-ray diffraction pattern of the single crystal (figure 1(b)) is consistent with this structural model. The clear c-axis orientation of the crystal surface is revealed by the (00l) diffraction peaks. The accurate thickness was measured by atomic force microscope (AFM) to make it correspond to different contrasts under an optical microscope, so that the approximate thickness of subsequent samples can be judged by contrast. This method has been successfully used in the characterization of graphene [35]. In figures 1(d)–(f), we present the optical image, AFM image and the cross-sectional profile of a typical exfoliated sample, which shows a thickness of 25 nm. More images with different contrasts and thicknesses can be seen in the supplementary information (SI). Due to the quick deterioration of the ultrathin samples in air, it is currently difficult to obtain the intrinsic properties in samples thinner than 15 nm. In this work, electrical transport measurements are carried out on two samples

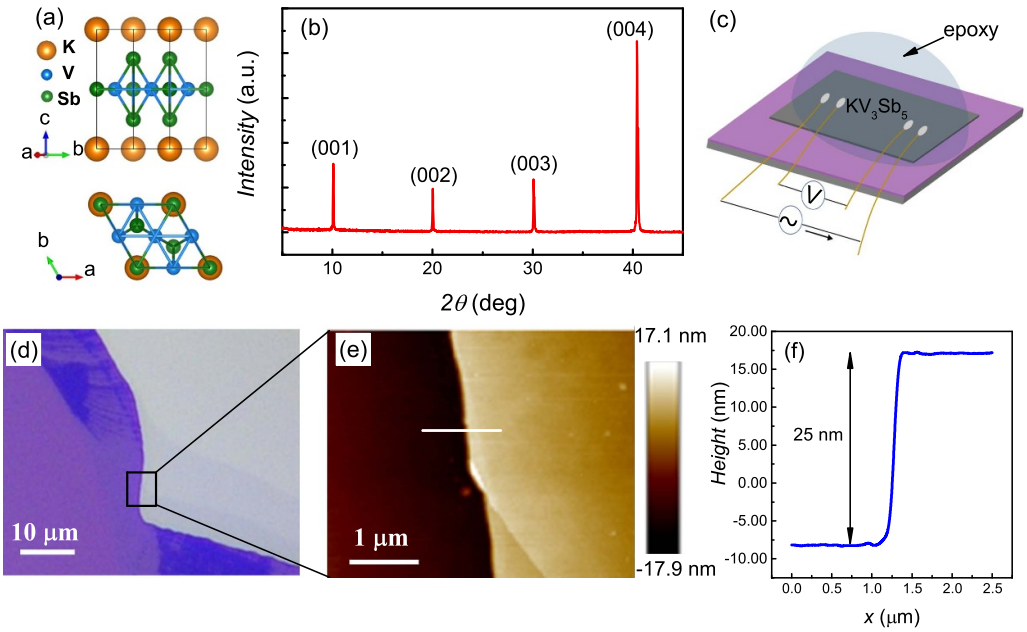

Figure 1. (a) Crystal structure of KV_3Sb_5 viewing from different directions. (b) X-ray diffraction pattern of the KV_3Sb_5 single crystal. (c) Schematic picture of the measurement set-up. Samples S-1 is not protected while S-2 is protected by epoxy. (d) A picture of the thin sample under optical microscope. (e) The Atomic force microscopy image of the area marked by the square in (d). (f) Cross-sectional profile of the thin sample along the white line in (e). The step is about 25 nm in height.

with the same thickness of 22 ± 2 nm (being equivalent to 25 layers of KV_3Sb_5), which are denoted as S-1 and S-2 respectively. Due to the degradation of the thin sample, the thickness of the samples used for electrical transport experiments cannot be measured using AFM, but was estimated by the contrast of the sample under an optical microscope. The relatively large error bar comes from the estimation process.

The temperature dependence of the resistance of the thin KV_3Sb_5 samples S-1 and S-2, along with that of the bulk sample, is shown in figure 2(a). The SC transition can be observed at low temperatures. The onset transition temperature T_c^{onset} (using the criterion of 90% R_n, R_n is the normal-state resistance before SC transition) is 1.23 K and 1.72 K for S-1 and S-2 respectively, which is higher than that of the bulk sample (~0.92 K). We note that the enhancement of T_c^{onset} reaches an extent as high as 87% for sample S-2. A similar enhancement of the superconductivity has been reported in the CsV_3Sb_5 system, which was interpreted as the result of hole doping by selective oxidation on the surface of the thin samples [34]. The difference of T_c^{onset} between S-1 and S-2 may originate from the different extent of the surface doping, since the two samples have different protection conditions. A slight doping process can increase T_c to a rather significant extent (S-2), while a heavier doping process will suppress the superconductivity (S-1). Moreover, when the thickness of the sample increases within a certain range (see figures S4(a) and (b)), T_c also shows a rising trend. This further reflects that the reduction of excessive hole doping in thick samples is beneficial for superconductivity.

We also found that the value of magnetoresistance of the thin sample S-2 is suppressed down to about a tenth as compared with the bulk sample (see figure S4(e) in the SI), which indicates that the electronic structure is really affected by reducing the sample thickness and the accompanied doping effect. We note that, besides the doping effect, a clear enhancement of the disorder level is also induced in the process of mechanical exfoliation. The residual resistance ratio, which reflects the degree of impurity and/or disorder, decreases from about 29.85 ± 0.14 in the bulk samples to 5.57 ± 0.05 (S-1) and 6.51 ± 0.02 (S-2) in the thin samples. Sample S-1 is more disordered than S-2, being consistent with the different protection conditions of the two samples.

3.2. BKT transition

Despite the difference in the SC transition temperature, the two thin samples reveal similar broad SC transitions in the *R-T* curves as compared to the bulk sample and show a tail-like feature in a wide temperature range. Similar behaviors have been reported in other 2D SC materials, which were explained in terms of the BKT transition [7, 13, 37]. Based on this picture, the zero-resistance state is driven by the binding of vortex–antivortex pairs and the resistance can be described by the equation [37, 38],

$$R = R_0 \exp\left[-b\left(\frac{T}{T_{\text{BKT}}} - 1\right)\right]^{-1/2}. \quad (1)$$

As shown by the dashed lines in figure 2(a), the consistence between the resistance data and the fitting curve demonstrates the occurrence of BKT transition in the thin samples. The BKT

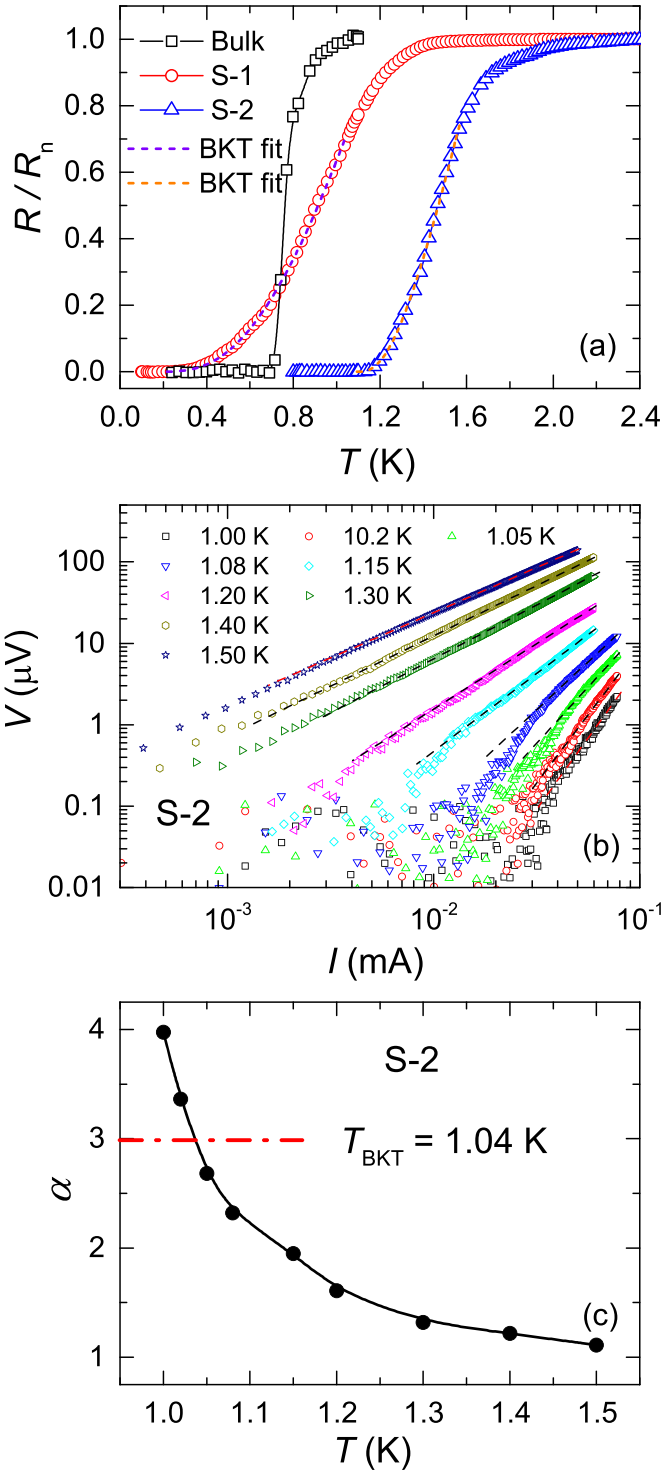

Figure 2. (a) Temperature dependence of resistance of two KV_3Sb_5 thin films at zero magnetic field. The data of the bulk sample is also shown for comparison. The dashed lines are the fitting curves representing the BKT transition (see text). (b) *V*–*I* curves at different temperatures for the sample S-2. The dashed line are the results of the power-law fitting using the equation $V \sim I^{\alpha}$. (c) The exponent α versus *T* extracted from the fitting.

transition temperature is determined to be $T_{BKT} = 0.08$ K and 1.06 K for S-1 and S-2 respectively.

In order to further confirm the occurrence of the BKT transition, we checked the voltage–current (*V*–*I*) curves. As shown in figure 2(b), the *V*–*I* curves of sample S-2 all show the power-law behavior, $V \sim I^{\alpha}$, at different temperatures. It is known that a universal relation $V \sim I^3$ should be obeyed at the BKT transition point. In the inset of figure 2(b), we show the temperature dependence of the exponent α, from which the transition point T_{BKT} is determined to be 1.04 K. This value is very close to that obtained from fitting the $R - T$ curve. The BKT-type behavior suggests that 2D superconductivity is achieved at zero magnetic field in the thin samples.

3.3. AM and thermally activated flux flow (TAFF) behaviors

Next, we focus on the electrical transport behavior under the out-of-plane magnetic fields. As shown in figures 3(a) and (b), the *R*–*T* curves show a systematic evolution with the increase in field. For sample S-1, the zero-resistance state is destroyed by a magnetic field as low as 50 Oe, suggesting a very narrow SC region. While for sample S-2, the zero-resistance state can be maintained at fields up to 600 Oe (an enlarged view can be seen in figure S5 in SI). Above the zero-resistance state, for both samples, a temperature-independent resistance is observed in a wide field range in the low temperature region. In order to further understand this unconventional temperature-independent behavior of the *R*–*T* curves, we plot the Arrhenius plots (ln*R* vs $1/T$) of S-1 under several typical fields in figure 3(c) (the data of S-2 is shown in figure S6 in SI). Ln*R* shows a transformation from the linear evolution to the $1/T$-independent tendency with the increase of $1/T$, which are represented by the dashed and dotted lines respectively. The intersections of the dashed and dotted lines are used to determine the transition points between the two behaviors.

The linear relation is the consequence of the TAFF behavior, where $R(T)$ obeys the relationship [39, 40]

$$R(T) = R_0 \exp\left(-\frac{U}{k_B T}\right). \tag{2}$$

Here k_B is the Boltzmann constant and *U* is the thermally activated energy of the flux flow. In fact, the TAFF behavior reflects the motion characteristics of the flux vortex under the influence of thermal activation in the flux liquid region. Theoretically, it was pointed out in references [41, 42] that the activation energy is determined by the free energy barriers to create a single free dislocation when the vortex translational correlation length is small enough. Such a behavior has been observed in other systems, including Fe-based superconductors [43, 44], cuprates [39, 45–47] and transition metal disulphides [40]. The value of $U(H)$ can be obtained from the slope of the linear part of the Arrhenius plot. The acquired $U(H)$ at various magnetic fields for samples S-1 and S-2 are summarized in figure 3(d). Although sample S-1 shows smaller activation energy in the low field region, it exhibits a more gradual decline trend with increasing magnetic field, and overwhelms the *U* value of sample S-2 near 1.2 kOe. This most likely reflects the fact that there are more flux pinning centers in the sample S-1, thus effectively pinning the flux even when the flux density is high in the high field region. This result is consistent with the above statement that the sample S-1 has a higher degree of disorder as compared with sample S-2.

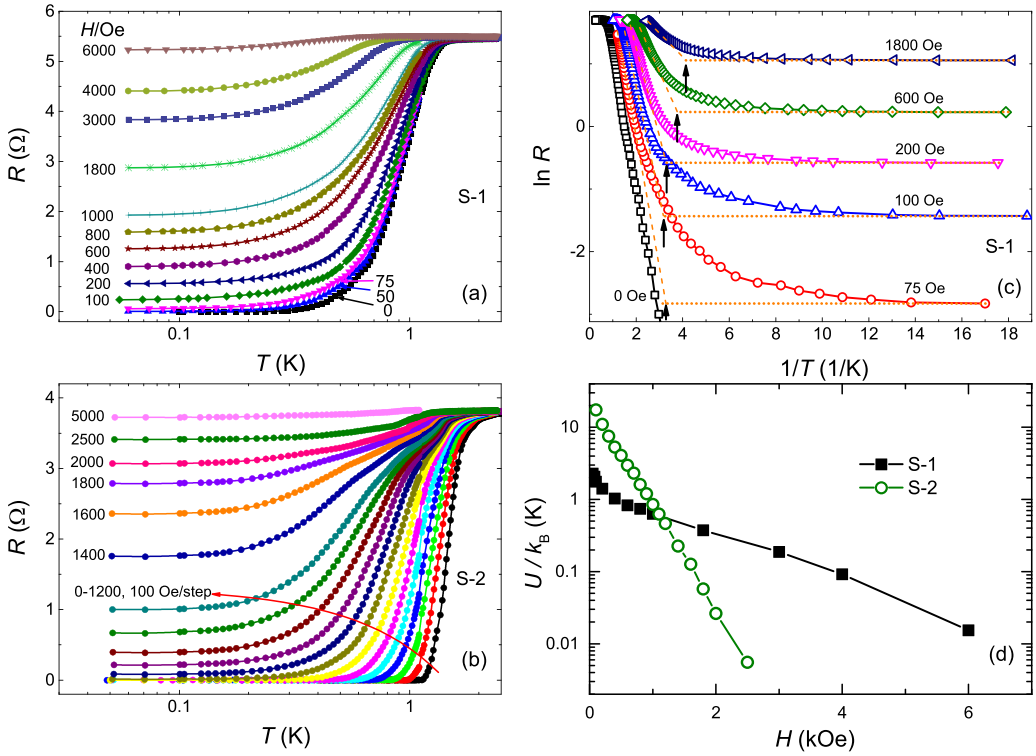

Figure 3. (a) and (b) Electrical resistance as a function of temperature under different out-of-plane magnetic fields ($H \parallel c$) for samples S-1 and S-2 respectively. (c) Arrhenius plots of longitudinal resistivity ln$R$ vs $1/T$ under different fields for the sample S-1. The data are shifted rightward by 0.3 K^{-1} for clarity. The dashed lines are the fits with TAFF theory to the experimental data. The dotted horizontal lines are guides for eyes. The arrows indicate the transition points between the two regions with different behaviors. (d) Field dependence of thermally activated energy U for samples S-1 and S-2.

With the increase of $1/T$, the resistance becomes constant, which is independent of temperature. Such a metallic state in the vicinity of the SC region could not be understood in the classical framework. Similar phenomena have been reported in other 2D SC systems and are considered as a hallmark of the AM state [5–10]. The physical origin of this AM state is still debated. As we have stated in the introduction, the quantum tunneling of vortices [18] and Bose metallic phase [5, 19] are the two main theoretical pictures to explain the AM state.

We should be very careful when investigating the AM state, which typically emerges in the ultra-low temperature region. Firstly, the electron–phonon interaction is very weak at ultra-low temperatures. In this case, high-frequency noise from the measurement instruments and environment may exert a great influence, which causes the electron temperature to elevate from the lattice temperature [10, 48, 49]. Thus, an effective filtering is necessary to carry out the transport measurements in this temperature region. In our experiments, all the transport data are obtained with the RC filters installed at room temperature. As can be seen in figure S7 in the SI, the use of RC filters significantly improves the performance of the data at ultra-low temperatures. Secondly, it was found that the magnitude of current can also affect the behavior of the resistance in low-dimensional systems [50]. In this work, the current of around 5–10 μA is used in the transport measurements. Considering the relatively large transverse dimension (∼200 μm) and thickness (∼22 nm), which results in a cross sectional area about 210 times larger than that in reference [10], the current density is about 1–2 μA μm^{-2}. Although the magnitude of current density is slightly larger than that used by Xing *et al* [10], in a relatively small magnetic field (e.g. 800 Oe for sample S-2), the saturated resistance is in the order of 0.1 Ω. Thus, at least for lower levels of the saturated resistance, the voltage drop and Joule heat on the sample is small, and the data is reliable.

4. Discussion

Based on the above observations, we can draw the field-temperature phase diagram of the two thin KV_3Sb_5 samples, which is shown in figures 4(a) and (b). The colormap of the derivative of the resistance to temperature reveals the distinguishable features of different states. The upper boundary of the SC state is determined by the zero-resistance points as shown by the arrowed lines in figure S5. For sample S-1, a true zero-resistance state is not observed under the lowest field of our experiment, 50 Oe. Thus, we did not indicate the SC region in this diagram. As for S-2, a clear zero-resistance SC region is presented in this phase diagram. The criteria for determining the boundary between the AM and TAFF regions are shown by the black arrows in figure 3(c). A remarkable feature of the two phase diagrams is that the boundary between the AM and TAFF states is rather steep in a wide field range, revealing the robustness of the AM state against the magnetic field.

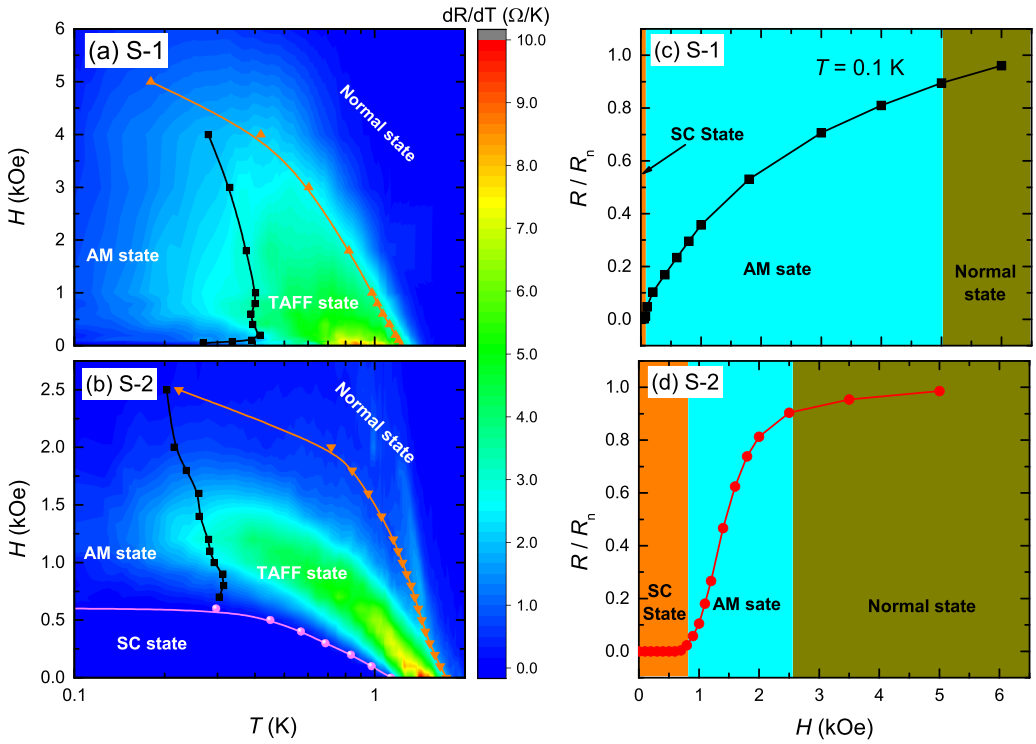

Figure 4. Phase diagram for the KV_3Sb_5 thin films S-1 (a) and S-2 (b). Different states can be distinguished clearly by the derivative of resistance to temperature. The boundary between the TAFF and normal states is determined from the $R-T$ data using the criterion of 90% R_n. The criterion for determining the boundary between the AM and TAFF states is indicated by the black arrows shown in figure 3(c). The SC state in (b) represents the zero-resistance state (the details for determining the zero-resistance points can be seen in SI). (c) and (d) Field dependence of the normalized resistance (R/R_n) at 0.1 K for the two samples S-1 and S-2 respectively. The regions of SC, AM, and normal states are revealed by different colors.

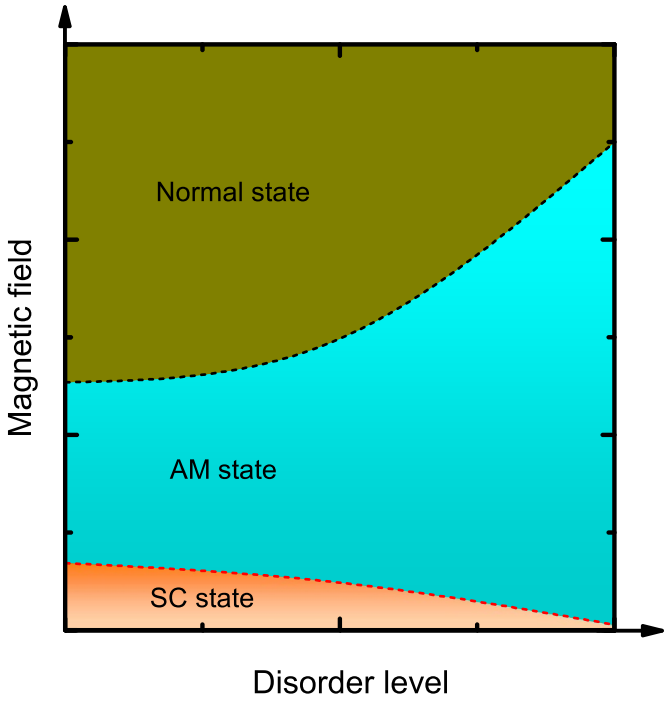

Figure 5. A schematic diagram of the competition between superconducting and AM states under the control of disorder level.

Moreover, we would like to point out that the field boundary between the TAFF and normal states exceeds the upper critical field of the bulk sample [25] by 10 and 5 times for sample S-1 and S-2 respectively. The origin of such unconventional observations, especially the possible correlation to the exotic electronic structure, is a very important topic for the theoretical realm in the future.

Finally and most importantly, a careful comparison between samples S-1 and S-2 can provide crucial information about the relation between the SC and AM states in low dimensions. Sample S-1 shows a relatively lower SC transition temperature (both the onset and zero-resistance points) under zero field. In addition, the zero-resistance state in S-1 is more fragile against the magnetic field than S-2, revealing a very narrow SC region in the R/R_n-H space as shown in figure 4(c). In sharp contrast, the AM state of sample S-1 spreads to a rather large area up to 5 kOe, which is about 2 times of that of sample S-2 (see figure 4(d)). We note again that sample S-1 was exposed in air for a longer time than S-2, since the latter was protected by epoxy after the fabrication of electrodes. As the experiments indicate, the stronger degradation process endured by S-1 has weakened its superconductivity. Meanwhile, the AM state in sample S-1 is more tenacious against the magnetic field. In this sense, our results definitely unveil the competitive relationship between the SC and AM states. Such an evolution of the three states—SC state, AM state, and normal state—is displayed schematically in figure 5.

Although the physical mechanism behind this evolutionary behavior is not yet fully understood, we can still see some important clues. First of all, sample S-1 with higher disorder shows a lower T_c and the zero-resistance state reveals a greater

fragility against the applied magnetic fields. This is reasonable, and actually reflects the general characteristics of low-dimensional superconductivity. On the other hand, the robustness of AM states under high magnetic fields in the high-disorder side of figure 5, is reminiscent of the fact that the upper critical field of a dirty-limit superconductor is inversely proportional to the mean free path of quasi-particles [51, 52]. This implies that there is some intrinsic similarity between the mechanisms by which the AM state disappears under a magnetic field and the traditional destruction of the SC state under the upper critical field.

5. Conclusion

In summary, we successfully obtained SC thin flakes of the Kagome metal KV_3Sb_5 with the thickness down to 22 ± 2 nm by using a mechanical exfoliation method. The dimensionality effect was observed in terms of the higher onset SC transition temperature and the BKT-type resistance transition. Most intriguing of all, a competitive relationship between the SC and AM states is uncovered by the comparative study of the field tuned phase diagram of the two thin samples with different levels of disorder. Our results provide very clear information about the interplay between the SC and AM states in low dimensions.

Data availability statement

All data that support the findings of this study are included within the article (and any supplementary files).

Acknowledgments

This work is supported by the National Natural Science Foundation of China (Nos. 11204338 and 51925208), the Strategic Priority Research Program of Chinese Academy of Sciences (Grant No. XDB30000000), talents plan launch funding of Zhejiang University of Technology (Grant No. 202241637029), and Research funding of Institute for Frontiers and Interdisciplinary Sciences of Zhejiang University of Technology.

ORCID iDs

Aobo Yu https://orcid.org/0000-0003-4538-8478
Wei Peng https://orcid.org/0000-0002-9888-1891
Zengfeng Di https://orcid.org/0000-0002-9357-5107
Fuqiang Huang https://orcid.org/0000-0003-0526-5473
Da Jiang https://orcid.org/0000-0002-4341-2289
Gang Mu https://orcid.org/0000-0001-5676-4702

References

[1] de la Barrera S C *et al* 2018 *Nat. Commun.* **9** 1427
[2] Xi X, Wang Z, Zhao W, Park J-H, Law K T, Berger H, Forro L, Shan J and Mak K F 2016 *Nat. Phys.* **12** 139
[3] Lu J M, Zheliuk O, Leermakers I, Yuan N F Q, Zeitler U, Law K T and Ye J T 2015 *Science* **350** 1353
[4] Saito Y, Nojima T and Iwasa Y 2016 *Nat. Rev. Mater.* **2** 16094
[5] Phillips P and Dalidovich D 2003 *Science* **302** 243
[6] Ephron D, Yazdani A, Kapitulnik A and Beasley M R 1996 *Phys. Rev. Lett.* **76** 1529
[7] Saito Y, Kasahara Y, Ye J, Iwasa Y and Nojima T 2015 *Science* **350** 409
[8] Qin Y, Vicente C L and Yoon J 2006 *Phys. Rev.* B **73** 100505
[9] Yang C *et al* 2019 *Science* **366** 1505
[10] Xing Y *et al* 2021 *Nano Lett.* **21** 7486
[11] Berezinskii V L 1971 *Sov. Phys. JETP* **32** 493
[12] Kosterlitz J M and Thouless D J 1973 *J. Phys.* C*: Solid State Phys.* **6** 1181
[13] Reyren N *et al* 2007 *Science* **317** 1196
[14] Gozar A, Logvenov G, Kourkoutis L F, Bollinger A T, Giannuzzi L A, Muller D A and Bozovic I 2008 *Nature* **455** 782
[15] Wang Q-Y *et al* 2012 *Chin. Phys. Lett.* **29** 037402
[16] Pan J *et al* 2017 *J. Am. Chem. Soc.* **139** 4623
[17] Yang Y, Fang S, Fatemi V, Ruhman J, Navarro-Moratalla E, Watanabe K, Taniguchi T, Kaxiras E and Jarillo-Herrero P 2018 *Phys. Rev.* B **98** 035203
[18] Shimshoni E, Auerbach A and Kapitulnik A 1998 *Phys. Rev. Lett.* **80** 3352
[19] Das D and Doniach S 2001 *Phys. Rev.* B **64** 134511
[20] Norman M R 2016 *Rev. Mod. Phys.* **88** 041002
[21] Ma D-S, Xu Y, Chiu C S, Regnault N, Houck A A, Song Z and Bernevig B A 2020 *Phys. Rev. Lett.* **125** 266403
[22] Kiesel M L, Platt C and Thomale R 2013 *Phys. Rev. Lett.* **110** 126405
[23] Ortiz B R *et al* 2019 *Phys. Rev. Mater.* **3** 094407
[24] Ortiz B R *et al* 2020 *Phys. Rev. Lett.* **125** 247002
[25] Ortiz B R, Sarte P M, Kenney E M, Graf M J, Teicher S M L, Seshadri R and Wilson S D 2021 *Phys. Rev. Mater.* **5** 034801
[26] Yin Q, Tu Z, Gong C, Fu Y, Yan S and Lei H 2021 *Chin. Phys. Lett.* **38** 037403
[27] Wu X *et al* 2021 *Phys. Rev. Lett.* **127** 177001
[28] Chen K Y *et al* 2021 *Phys. Rev. Lett.* **126** 247001
[29] Chen X, Zhan X, Wang X, Deng J, Liu X-B, Chen X, Guo J-G and Chen X 2021 *Chin. Phys. Lett.* **38** 057402
[30] Wang Q *et al* 2021 *Adv. Mater.* **33** 2102813
[31] Zhu C C *et al* 2022 *Phys. Rev.* B **105** 094507
[32] Liang Z *et al* 2021 *Phys. Rev.* X **11** 031026
[33] Xiang Y, Li Q, Li Y, Xie W, Yang H, Zhiwei W, Yao Y and Wen H 2021 *Nat. Commun.* **12** 6727
[34] Song Y, Ying T, Chen X, Han X, Wu X, Schnyder A P, Huang Y, Guo J-G and Chen X 2021 *Phys. Rev. Lett.* **127** 237001
[35] Novoselov K S, Geim A K, Morozov S V, Jiang D, Zhang Y, Dubonos S V, Grigorieva I V and Firsov A A 2004 *Science* **306** 666
[36] Jiang D *et al* 2014 *Nat. Commun.* **5** 5708
[37] Xu C, Wang L, Liu Z, Chen L, Guo J, Kang N, Ma X-L, Cheng H-M and Ren W 2015 *Nat. Mater.* **14** 1135
[38] Halperin B I and Nelson D R 1979 *J. Low Temp. Phys.* **36** 599
[39] Vinokur V M, Feigel'man M V, Geshkenbein V B and Larkin A I 1990 *Phys. Rev. Lett.* **65** 259
[40] Zhang H, Fang Y, Wang T, Liu Y, Chu J, Li Z, Jiang D, Mu G, Di Z and Huang F 2021 *Phys. Rev.* B **103** L180503
[41] Feigel'man M, Geshkenbein V and Larkin A 1990 *Physica* C **167** 177
[42] White W R, Kapitulnik A and Beasley M R 1993 *Phys. Rev. Lett.* **70** 670
[43] Xing X, Yi X, Li M, Meng Y, Mu G, Ge J-Y and Shi Z 2020 *Supercond. Sci. Technol.* **33** 114005
[44] Liu Y, Wang T, Xu Z, Hong W, Peng W, Lin Z-R, Luo H and Mu G 2023 *Supercond. Sci. Technol.* **36** 095008

[45] Zou X, Wang Z, Chen J and Zhang H 2001 *Physica* C **356** 31
[46] Brunner O, Antognazza L, Triscone J-M, Miéville L and Fischer O 1991 *Phys. Rev. Lett.* **67** 1354
[47] Qiu X G, Wuyts B, Maenhoudt M, Moshchalkov V V and Bruynseraede Y 1995 *Phys. Rev.* B **52** 559
[48] Tamir I *et al* 2019 *Sci. Adv.* **5** eaau3826
[49] Wang P, Huang K, Sun J, Hu J, Fu H and Lin X 2019 *Rev. Sci. Instrum.* **90** 023905
[50] Benyamini A *et al* 2019 *Nat. Phys.* **15** 947–53
[51] Helfand E and Werthamer N R 1966 *Phys. Rev.* **147** 288
[52] Rainer D and Bergmann G 1974 *J. Low Temp. Phys.* **14** 501